

Searching for Compact Object Candidates from LAMOST Time-Domain Survey of Four K2 Plates

SENYU QI,¹ WEI-MIN GU,¹ TUAN YI,¹ ZHI-XIANG ZHANG,¹ SONG WANG,² AND JIFENG LIU^{2,3}

¹*Department of Astronomy, Xiamen University, Xiamen, Fujian 361005, China*

²*National Astronomical Observatories, Chinese Academy of Sciences, Beijing 100101, China*

³*College of Astronomy and Space Science, University of Chinese Academy of Sciences, Beijing 100101, China*

ABSTRACT

The time-domain (TD) surveys of the Large Sky Area Multi-Object Fiber Spectroscopic Telescope (LAMOST) yield high-cadence radial velocities, paving a new avenue to study binary systems including compact objects. In this work, we explore LAMOST TD spectroscopic data of four K2 plates and present a sample of six single-lined spectroscopic binaries that may contain compact objects. We conduct analyses using phase-resolved radial velocity measurements of the visible star, to characterize each source and to infer the properties of invisible companion. By fitting the radial velocity curves for the six targets, we obtain accurate orbital periods, ranging from $\sim (0.6\text{--}6)$ days, and radial velocity semi-amplitudes, ranging from $\sim (50\text{--}130)$ km s⁻¹. We calculate the mass function of the unseen companions to be between 0.08 and 0.17 M_{\odot} . Based on the mass function and the estimated stellar parameters of the visible star, we determine the minimum mass of the hidden star. Three targets, J034813, J063350, and J064850, show ellipsoidal variability in the light curves from K2, ZTF, and *TESS* surveys. Therefore, we can put constraints on the mass of the invisible star using the ellipsoidal variability. We identify no X-ray counterparts for these targets except for J085120, of which the X-ray emission can be ascribed to stellar activity. We note that the nature of these six candidates is worth further characterization utilizing multi-wavelength follow-up observations.

Keywords: Close binary stars (254), Compact objects (288), Light curves (918), Radial velocity (1332)

1. INTRODUCTION

White dwarfs (WDs), neutron stars (NSs), and black holes (BHs) are remnants of stars that ended their lifetimes. The identification and characterization of these objects can yield key insights into strong gravitational fields, stellar formation, evolution history, binary interactions and evolution, and the properties and behavior of matter at extreme densities. Additionally, compact objects are closely related to various astronomical phenomena, such as novae, kilonovae, supernovae, X-ray bursts, gamma-ray bursts (Troja et al. 2022), and gravitational waves. Many observations show that more than half of stars in the Galaxy are in binary systems (Duchêne & Kraus 2013) and that binary systems con-

tain a substantial number of compact objects (Remillard & McClintock 2006; Joss & Rappaport 1984; Rebassa-Mansergas et al. 2012).

The number of binaries including WDs has skyrocketed in recent years, thanks to state-of-the-art time-domain surveys (Rebassa-Mansergas et al. 2016; Parsons et al. 2016; Ren et al. 2018; El-Badry et al. 2021a; Rebassa-Mansergas et al. 2021; Zhang et al. 2022; Zheng et al. 2022a). The identification of the majority of the white dwarf–main-sequence (WD-MS) binaries relies on the distinctive spectral characteristics of WDs. And the majority of binary systems containing NSs or stellar-mass BHs are discovered by their bright bursts in the X-ray band (Kreidberg et al. 2012; Casares et al. 2014; Corral-Santana et al. 2016). The X-ray outbursts are caused by mass transfer from the companion overflowing the Roche lobe or stellar wind coming from the companion. Recent gravitational wave detection has confirmed some compact object binaries (Abbott et al. 2016, 2017, 2020). However, these sources only account for a small

Corresponding author: Wei-Min Gu, Tuan Yi, Zhi-Xiang Zhang
guwm@xmu.edu.cn
yit@xmu.edu.cn
zhangzx@xmu.edu.cn

population of total compact object binaries. Stellar evolution theory predicts that there are about $\sim 10^8$ stellar-mass BHs and $\sim 10^9$ NSs in our Milky Way (Brown & Bethe 1994). This indicates that there are still plenty of undiscovered quiescent dark objects in our galaxy.

One promising strategy for discovering more dormant compact objects is to search for single-lined spectroscopic binary systems with large mass functions. The methodology, commonly known as the dynamical method, utilizes multi-epoch spectroscopic observations to monitor stars with large radial velocity variations potentially induced by a compact companion. Dynamical searches for non-interacting BHs binaries and NSs binaries (Trimble & Thorne 1969) commenced even before the identification of the first BH in X-ray binaries. Recently, a couple of stellar-mass BHs and NSs in binary systems have been discovered based on the dynamical method (Thompson et al. 2019; Liu et al. 2019, 2020; Jayasinghe et al. 2021; El-Badry et al. 2022; Yi et al. 2022; Zheng et al. 2022b; El-Badry et al. 2023). Using time-domain (TD) spectroscopic, astrometric, and photometric surveys, the orbital parameters of the systems and the stellar properties of the optically visible stars can be determined, and the presence of hidden companions can be dynamically confirmed.

The Large Sky Area Multi-Object Fiber Spectroscopic Telescope (LAMOST) is a reflecting Schmidt telescope with a four-meter effective aperture and a wide field of view (Cui et al. 2012). LAMOST provides millions of stellar spectra in both medium-resolution mode ($R \sim 7500$) and low-resolution mode ($R \sim 1800$). LAMOST’s observation strategy of taking multiple spectra for individual targets provides an ideal opportunity to search for binary systems containing compact objects by dynamical methods. Furthermore, numerous ground- or space-based photometric surveys are now providing vast quantities of photometric data, which include the *Kepler* K2 mission (Howell et al. 2014), the Zwicky Transient Facility (ZTF; Bellm et al. 2019), the All-Sky Automated Survey for Supernovae (ASAS-SN; Shappee et al. 2014) and Transiting Exoplanet Survey Satellite (*TESS*; Ricker et al. 2015). The high-cadence photometry has the potential to be an effective means for searching for compact object candidates (Rowan et al. 2021; Gomel et al. 2021, 2022). Utilizing the TD spectroscopic data from LAMOST and the wealth of photometric data from ground- or space-based surveys, a dozen of compact object candidates have been revealed (Gu et al. 2019; Zheng et al. 2019; Yang et al. 2021; Mu et al. 2022; Li et al. 2022; Mazeh et al. 2022; Yuan et al. 2022).

This paper aims to search for compact objects in binary systems based on the LAMOST TD spectroscopic

data of four K2 plates (Wang et al. 2021, see their Figure 1). We select a sample containing six single-lined spectroscopic binaries which all have more than 20 radial velocity measurements. We determine the orbital parameters from radial velocity curves and light curves. Then the mass of the optically invisible stars in binaries is estimated by using the mass function. We introduce the details of the data and the criterion for selecting candidates in Section 2. The properties of the sample are shown in Section 3, including the orbital parameters and the stellar parameters. The discussion and the summary are presented in Section 4 and Section 5, respectively.

2. DATA SELECTION

2.1. Data

From Oct. 2019 to Apr. 2020, LAMOST conducted a TD survey to observe four footprints (fields) of the K2 campaign (Wang et al. 2021, we refer to the survey as four K2 plates). The survey extends the achievements of the LAMOST-Kepler/K2 projects conducted TD and non-TD sky surveys covering the Kepler field and the K2 campaigns from 2012 to 2019 (Fu et al. 2020; Zong et al. 2020). The four K2 plates have collected $\sim 767,000$ low-resolution and $\sim 478,000$ median-resolution spectra. Wang et al. (2021) used different methods, including the LAMOST Stellar Parameter Pipeline (LASP), the DD-Payne, and the Stellar LABEL Machine (SLAM) to determine the stellar parameters, namely, effective temperature, surface gravity, metallicity, and radial velocity. We select 7245 sources from the sample with multiple medium-resolution observations and a mean signal-to-noise ratio (SNR) greater than 10. In our sub-sample, 5468 sources have more than 10 medium-resolution exposures and 4121 sources have more than 20 exposures. All these data are available in the LAMOST DR9¹.

2.2. Candidates Selection

Compact object candidates can be selected using the mass function:

$$f(M_2) \equiv \frac{M_2^3 \sin^3 i}{(M_1 + M_2)^2} = \frac{K_1^3 P_{\text{orb}}}{2\pi G}, \quad (1)$$

where M_1 is the mass of the optically visible star and M_2 is the mass of the invisible companion, K_1 is the radial velocity semi-amplitude of the visible star, P_{orb} is the orbital period, i is the orbital inclination angle, and G is the gravitational constant. The mass function is

¹ <http://www.lamost.org/dr9/v1.0/catalogue>

Table 1. Basic information for the sources in our sample.

ID	R.A.	Decl	ϖ	gmag
	(J2000)	(J2000)	(mas)	(mag)
J034813	57.055792	25.098805	1.168 ± 0.013	12.24
J063350	98.459806	22.015557	0.304 ± 0.026	14.54
J064717	101.822211	24.609382	0.399 ± 0.020	13.96
J064850	102.209808	24.830386	0.711 ± 0.018	13.89
J085102	132.758841	11.817029	1.280 ± 0.048	13.17
J104734	161.894238	7.923628	1.729 ± 0.015	13.15

NOTE—Column (1): designation of the source; column (2): R.A. (J2000); column (3): Decl.(J2000); column (4): parallax from *Gaia* DR3; column (5): g-band magnitude from *Gaia* DR3.

a stringent lower mass limit for the unseen companion when $i = 90^\circ$ and $M_1 = 0M_\odot$. K_1 and P_{orb} can be measured by fitting the radial velocity curve and the light curve. To find promising compact object candidates, we want sources with large mass functions. It is then obvious from Equation (1) that sources with either (or both) large K_1 or P_{orb} are favored.

According to previous research on binary systems containing compact objects, such as some stellar-mass BH binaries, a high proportion of the companion stars in these systems exhibit large radial velocity changes (Corral-Santana et al. 2016). And the distribution of their orbital periods ranges from a few hours to tens of days (Steehns et al. 2013; Corral-Santana et al. 2013).

In the first phase, we pick sources that have $\Delta V_R \gtrsim 80 \text{ km s}^{-1}$ and $\text{SNR} \geq 10$, where ΔV_R is the largest radial velocity variation among all spectroscopic data for a given source. Then we use the Lomb-Scargle algorithm (Lomb 1976; Scargle 1981) to search for periodic signals from the radial velocity measurements. The period corresponding to the highest Lomb-Scargle power is used to phase-fold the radial velocity curve. We visually inspect each radial velocity curve, discard poorly folded curves (e.g., sources with no significant periodic variation), and retain a sample of well-folded curves.

Note that each of our sources has got covered by at least 20, up to 60 repeating spectroscopic observations, ensuring that the radial velocity measurements encompass most of the orbital phases. Therefore, $\Delta V_R/2$ is a good approximation of K_1 and is used to estimate the mass function. Based on the $\Delta V_R/2$ and the period, we evaluate the mass functions by using Equation (1) and select the sources with $f(M_2) \gtrsim 0.1M_\odot$.

After that, we check if the spectrum of each source is single-lined. If a source has a single-lined spectrum but an apparent radial velocity variation, an unseen star that is either a compact object or a much fainter

star may exist in this binary system. We employ the method (Merle et al. 2017; Li et al. 2021) based on detecting multiple peaks of the cross correlation function (CCF) successive derivatives to determine double-lined (and multi-lined) spectroscopic systems (see Appendix). These non-single-lined spectroscopic binaries are removed from our sample.

Before reaching a final sample of candidates, we cross-match these sources with the K2 mission (Howell et al. 2014), ZTF (Bellm et al. 2019), ASAS-SN (Shappee et al. 2014), and *TESS* (Ricker et al. 2015). By using the light curves obtained from these surveys, we can exclude false positives such as close eclipsing binaries which obviously consist of two non-compact stars.

Finally, we gain a sample of six² single-lined spectroscopic binary with significant radial velocity variations as candidates who may host compact objects. Their basic information are presented in Table 1.

3. RESULTS

3.1. Radial velocity curves and mass functions

We measure the orbital periods from radial velocity measurements using two methods. As mentioned, first, we use the Lomb-Scargle method to search for the periodic signals from the radial velocity measurements. Second, we use *TheJoker* to fit the radial velocity curve. *TheJoker* is a python-based package that implements the Monte Carlo sampling technique to fit the two-body problem (Price-Whelan et al. 2017). A uniform period

² When assembling our sample, we found three compact object candidates have been proposed by Li et al. (2022) using the same LAMOST-K2 TD survey, therefore we do not include these three targets in our sample.

Table 2. Stellar parameters for the sources in our sample.

ID	P_{orb}	P_{ph}	K_1	e	R_1	T_{eff}	$\log g$	M_1	f	$f(M_2)$	M_2^{min}
	(day)	(day)	(km s^{-1})		(R_{\odot})	(K)	(dex)	(M_{\odot})	($\equiv R_1/R_{L1}$)	(M_{\odot})	(M_{\odot})
J034813	3.93	3.9289	61.72 ± 0.30	$0.002^{+0.002}_{-0.001}$	$3.19^{+0.16}_{-0.13}$	5440^{+65}_{-60}	$3.62^{+0.10}_{-0.09}$	$1.35^{+0.21}_{-0.16}$	$0.60^{+0.03}_{-0.04}$	0.096 ± 0.001	$0.75^{+0.07}_{-0.06}$
J063350	0.69	0.6934	133.22 ± 0.47	$0.069^{+0.006}_{-0.008}$	$2.36^{+0.09}_{-0.08}$	7644^{+80}_{-67}	$4.15^{+0.07}_{-0.07}$	$*1.74^{+0.20}_{-0.20}$	$*1.30^{+0.07}_{-0.07}$	0.170 ± 0.002	$1.11^{+0.07}_{-0.08}$
J064717	2.91	--	67.18 ± 0.40	$0.012^{+0.005}_{-0.005}$	$2.10^{+0.33}_{-0.17}$	6802^{+33}_{-33}	$3.93^{+0.07}_{-0.05}$	$1.43^{+0.23}_{-0.18}$	$0.47^{+0.04}_{-0.08}$	0.092 ± 0.002	$0.76^{+0.07}_{-0.06}$
J064850	1.23	1.2292	99.10 ± 0.64	$0.041^{+0.006}_{-0.005}$	$1.99^{+0.12}_{-0.11}$	5906^{+55}_{-48}	$3.96^{+0.09}_{-0.12}$	$1.09^{+0.12}_{-0.11}$	$0.87^{+0.06}_{-0.06}$	0.124 ± 0.002	$0.75^{+0.05}_{-0.05}$
J085102	5.78	--	53.57 ± 0.29	$0.003^{+0.003}_{-0.002}$	$1.46^{+0.10}_{-0.10}$	5880^{+23}_{-27}	$3.95^{+0.13}_{-0.06}$	$1.05^{+0.10}_{-0.06}$	$0.23^{+0.02}_{-0.02}$	0.092 ± 0.001	$0.64^{+0.04}_{-0.03}$
J104734	4.10	--	58.34 ± 0.31	$0.022^{+0.005}_{-0.005}$	$1.24^{+0.04}_{-0.04}$	5685^{+23}_{-40}	$4.24^{+0.06}_{-0.08}$	$0.91^{+0.05}_{-0.03}$	$0.26^{+0.01}_{-0.01}$	0.084 ± 0.001	$0.57^{+0.02}_{-0.01}$

NOTE—Column (1): designation of the source; column (2): orbital period from radial velocity curve; column (3): photometric period from light curve; column (4): semi-amplitude of radial velocity curve; column (5): eccentricity; column (6): radius measured by SED fitting; column (7): effective temperature measured by SED fitting; column (8): surface gravity measured by SED fitting; column (9): mass from the MIST model; column (10): filling factor. The * symbol denotes that the result $f > 1$ is non-physical (see discussion in Section 4.1); column (11): mass function; column (12): mass of the second star for $i = 90^\circ$.

prior spanning [0.1 d, 20 d] is set to for **TheJoker**. Consistent orbital periods are obtained from these two methods.

Following this, we derive the orbital parameters by fitting the radial velocity curve. We use the general form of a Keplerian orbit, that is: $V_r(t) = v_0 + K_1(\cos(f + w) + e \cos(w))$, where v_0 is the barycentric velocity (center-of-mass radial velocity), f is the true anomaly, w is the argument of periastron, and e is the eccentricity. The fitted radial velocity curves are shown in Figure 1 and the radial velocity semi-amplitudes are presented in Table 2. Then the mass function of each source is then calculated using Equation 1 and the results are also listed in Table 2. The fitting results reveal that the eccentricity of all sources is approximately equal to zero, indicating that the orbit is circularized.

3.2. Light curves

Meanwhile, we collect the light curves from various photometric TD surveys: K2, *TESS*, ZTF³, and ASAS-SN⁴. Light curves from K2 and *TESS* are obtained using the python package **Lightkurve** (Lightkurve Collaboration et al. 2018). We measure the photometric periods (P_{ph}) using the Lomb-Scargle algorithm. Three selected sources have a P_{ph} consistent with the orbital periods from the radial velocity curve fitting, and the phased-folded light curves are reliable based on our visual inspections (Figure 3). Their light curves show typical ellipsoidal modulation (a quasi-sinusoidal variation with double peaks and double valleys feature). The remaining three sources have no discernible periodic variations.

³ <https://irsa.ipac.caltech.edu/cgi-bin/Gator/nph-scan?projshort=ZTF&mission=irsa>

⁴ <https://asas-sn.osu.edu/variables>

3.3. Mass constraints

We use the broad-band spectral energy distributing (SED) fitting to constrain the stellar parameters of sources by using a python package **astroARIADNE**⁵. **AstroARIADNE** is designed as the program that uses the Nested Sampling algorithm to automatically fit the SED of target stars using as many as six distinct atmospheric model grids, to derive effective temperature, surface gravity, metallicity, distance, radius, and V-band extinction (Vines & Jenkins 2022).

We collect multi-band photometric data including GALEX (Martin et al. 2005; Bianchi et al. 2011), SDSS (Abazajian et al. 2009), APASS (Henden & Munari 2014), Pan-STARRS (Chambers et al. 2016), *TESS* (Ricker et al. 2015; Stassun et al. 2019), 2MASS (Skrutskie et al. 2006) and ALLWISE (Wright et al. 2010) to fit the SED. Then we use the parallax from *Gaia* DR3 (Gaia Collaboration et al. 2022) as the prior of distance. We derive the stellar parameters including T_{eff} , $\log g$, [Fe/H], and radius from the SED fitting, which are summarized in Table 2. Several SED fitting results are displayed in Appendix.

We use the stellar evolution models to evaluate the mass of visible companions by utilizing the python package **isochrones**⁶. We use the SED best-fit parameters and photometry as inputs to derive isochrone interpolated mass with MESA Isochrones & Stellar Tracks isochrones (MIST; Dotter 2016). The isochrone mass is shown in Table 2.

We adopt the isochrone mass as the mass of visible stars to constrain the mass of invisible companions. Combined with the mass function equation, the

⁵ <https://github.com/jvines/astroARIADNE>

⁶ <https://isochrones.readthedocs.io/en/latest/>

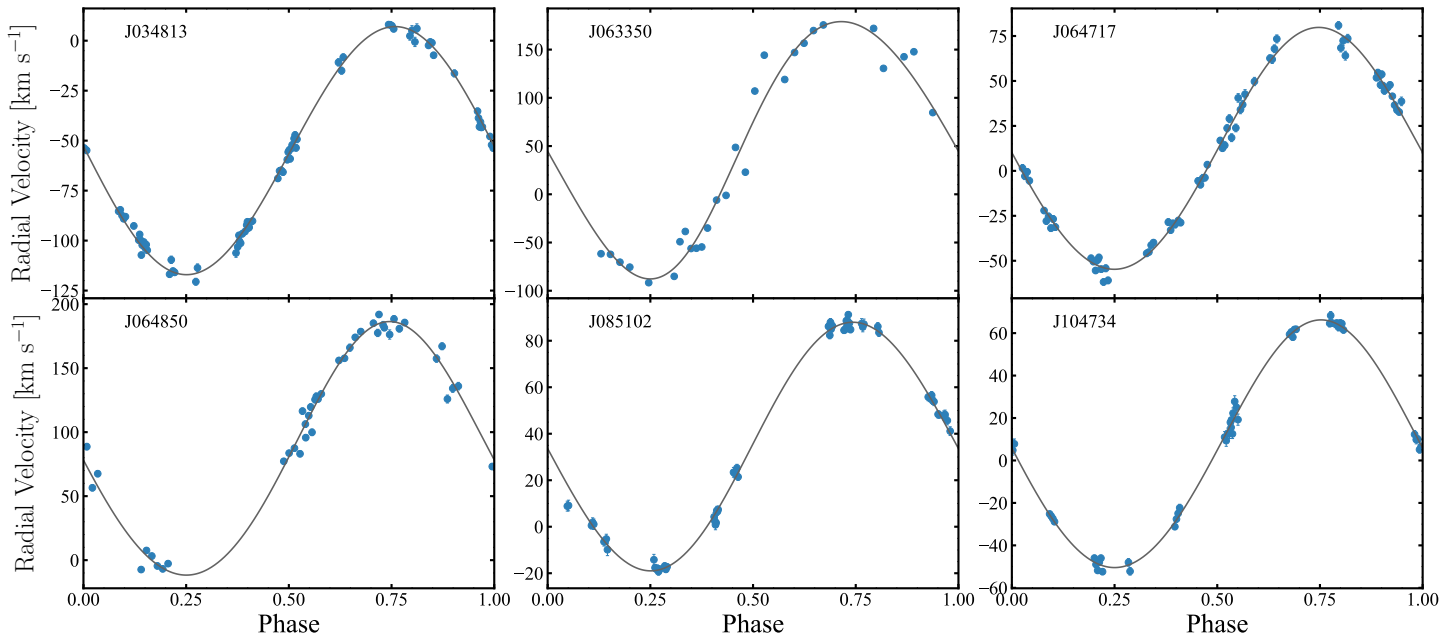


Figure 1. Phase-folded radial velocity data (dots) and the best-fitted radial velocity curves (lines) of the selected sources. The error bars for most data points are too small to be seen.

lower limit of the invisible object’s mass M_2^{\min} is calculated under the assumption that $i = 90^\circ$. We find that M_2^{\min} exceeds half of the visible stellar mass for all sources. Since a normal stellar companion of similar mass would contribute non-negligible optical flux and manifest double-lined spectroscopic features, the estimation indicates that each of the systems could conceal a compact object. The result is presented in the right panel of Figure 2.

4. DISCUSSION

4.1. Filling factor

Three of our chosen candidates exhibit standard ellipsoidal variability, whereas the remaining sources lack periodic photometric variability. After determining their binary orbital parameters and observable star parameters, we calculate the Roche lobe filling factor to characterize each system. The Roche lobe filling factor is defined as $f \equiv R_1/R_{L1}$, where the R_{L1} is the Roche lobe radius of the visible star. We express the R_{L1} as the form of (Paczynski 1971)

$$\frac{R_{L1}}{a} = 0.462 \left(\frac{M_1}{M_1 + M_2} \right)^{1/3}, \quad (2)$$

where a is the binary separation. The Kepler’s third law shows the relation between a and P_{orb} , which take the form as

$$\frac{G(M_1 + M_2)}{a^3} = \frac{4\pi^2}{P_{\text{orb}}^2}. \quad (3)$$

By combining the Equation (2) and the Equation (3) we obtain

$$\frac{M_1}{R_{L1}^3} = 0.804 P_{\text{day}}^{-2} \text{ g cm}^{-3}, \quad (4)$$

where P_{day} is the orbital period in the unit of days. We use Equation (4) to estimate R_{L1} . The filling factor is then estimated by $f \equiv R_1/R_{L1}$, where R_1 is measured from SED fitting. The results are listed in Table 2. The result is consistent in that sources with larger f exhibit significant periodic light curves, such as J034813 and J064850. Sources with small f are still far from filling their Roche lobe radii, therefore, they do not exhibit periodic photometric fluctuations.

The filling factor of J066350 is greater than 1, which is a non-physical picture since the Roche lobe radius cannot fall below the physical stellar radius. The photometric variability of J066350 reaches approximately 20% in amplitude, indicating that the optically visible star is close to or even fills up the Roche lobe. We suspect that the system has undergone a mass transfer process, and it may be inappropriate to estimate the stellar parameters by using stellar evolution models. We use $\log g$ values sampled by `astroARIADNE` to find that $M_1^{\text{grav}} = 10^{\log g R_1^2/G} = 2.8_{-0.7}^{+0.9} M_\odot$. In this case, the corresponding filling factor is around 0.94 to 1.22, suggesting that the mass uncertainty may be the cause of the $f > 1$ result and the parameters of this object could be physically consistent.

4.2. Constraining the invisible object’s mass

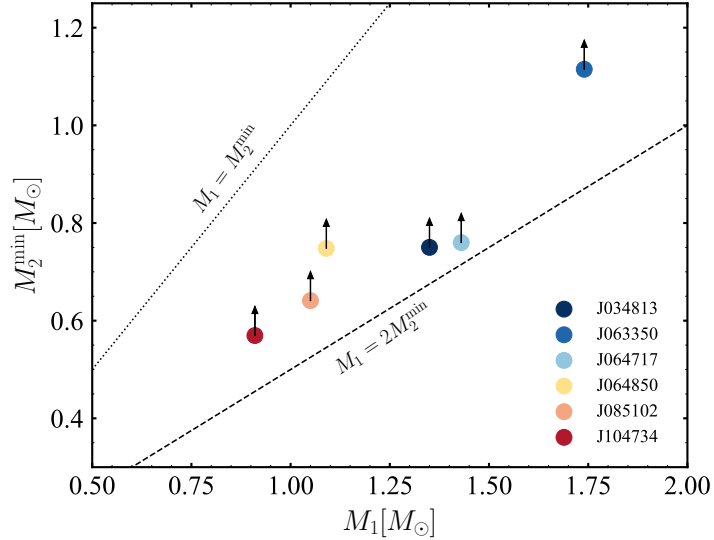


Figure 2. The minimum mass of the invisible companion M_2^{\min} at the maximum inclination ($i = 90^\circ$). Two dash lines represent the cases $M_1 = M_2^{\min}$ and $M_1 = 2M_2^{\min}$.

So far, we have only obtained a lower mass limit for the unseen component using the mass function, i.e., assuming that the orbital inclination $i = 90^\circ$. In this section, we make further constraints for the candidates showing ellipsoidal light curves.

The three selected candidates, J034813, J063350, and J064850, display typical ellipsoidal variability with a double-peaked profile. The cause of this variability is the tidal interaction between the binary system’s objects, which distorts the shape of the stars. The key factors that affect the ellipsoidal variability are the binary inclination angle i , the mass ratio $q = M_2/M_1$, the Roche lobe filling factor f , the limb-darkening coefficient, and the gravity-darkening coefficient. To determine the values of i and q , we utilize the PHOEBE 2.4 (Prša & Zwitter 2005; Prša et al. 2011; Conroy et al. 2020) software to fit the light curves. The procedures are outlined below.

When fitting the light curves, we keep the orbital period and effective temperature of the optically dominant star fixed at the values listed in Table 2. We set `distortion method = none` to model the invisible companion as an object without any contributions to flux or eclipses. The limb-darkening coefficients are derived from the PHOEBE atmosphere model with a logarithmic limb-darkening law. The gravitational darkening coefficient is treated as a free parameter and is assigned a prior of $\beta_1 \sim \mathcal{N}(0.32, 0.1)$ (see Claret & Bloemen 2011; El-Badry et al. 2021b). To perform the MCMC fitting, we use the radius and mass values provided in Table 2 as priors. We run multiple parallel chains using the `emcee` package (Foreman-Mackey et al. 2013), with each chain taking 10000 steps.

Figure 4 displays the posterior samples for q , i , and R_1 , while the best-fitting PHOEBE model results are illustrated by the red lines in Figure 3. A pure ellipsoidal model adequately fits the observed light curve. Our fitting results suggest $i = 55.36_{-13.73}^{+13.12}$ degree for J034813, with a corresponding invisible object mass of $M_2 = 0.98_{-0.20}^{+0.46} M_\odot$. The model indicates that the inclination of J063350 is nearly edge-on ($i = 84.81_{-5.27}^{+3.73}$ degree), leading to a $M_2 = 1.12_{-0.08}^{+0.10} M_\odot$. For J064850, $i = 50.82_{-10.99}^{+13.52}$ degree and $M_2 = 1.08_{-0.26}^{+0.46} M_\odot$.

4.3. The nature of six candidates

As mentioned in Section 4.2, for J034813, J063350, and J064813, we constrain the orbital inclinations by modeling the ellipsoidal light curves using PHOEBE. The results show that the invisible objects’ masses are around $1M_\odot$. Therefore, we propose that the three binaries contain a massive WD, although the possibility of an NS cannot be ruled out. For J064717, J085102, and J104734, the orbital inclination cannot be constrained due to the absence of periodic light curves; therefore, we calculate the minimum mass of their invisible object with $i = 90^\circ$. To constrain the inclination, one possible approach is to resolve the rotational broadening (Marsh et al. 1994) of the tidally locked visible star using high-resolution spectra.

We cross-match the candidates with available X-ray surveys: *Chandra* source catalog (Evans et al. 2010), *XMM-Newton* source catalog (Traulsen et al. 2020), *ROSAT* all-sky surveys (Voges et al. 1999) with a matching radius of $10''$. We do not find reported X-ray observations for most of the sources, except for J085102. An X-ray source 2CXO J085102.0+114901

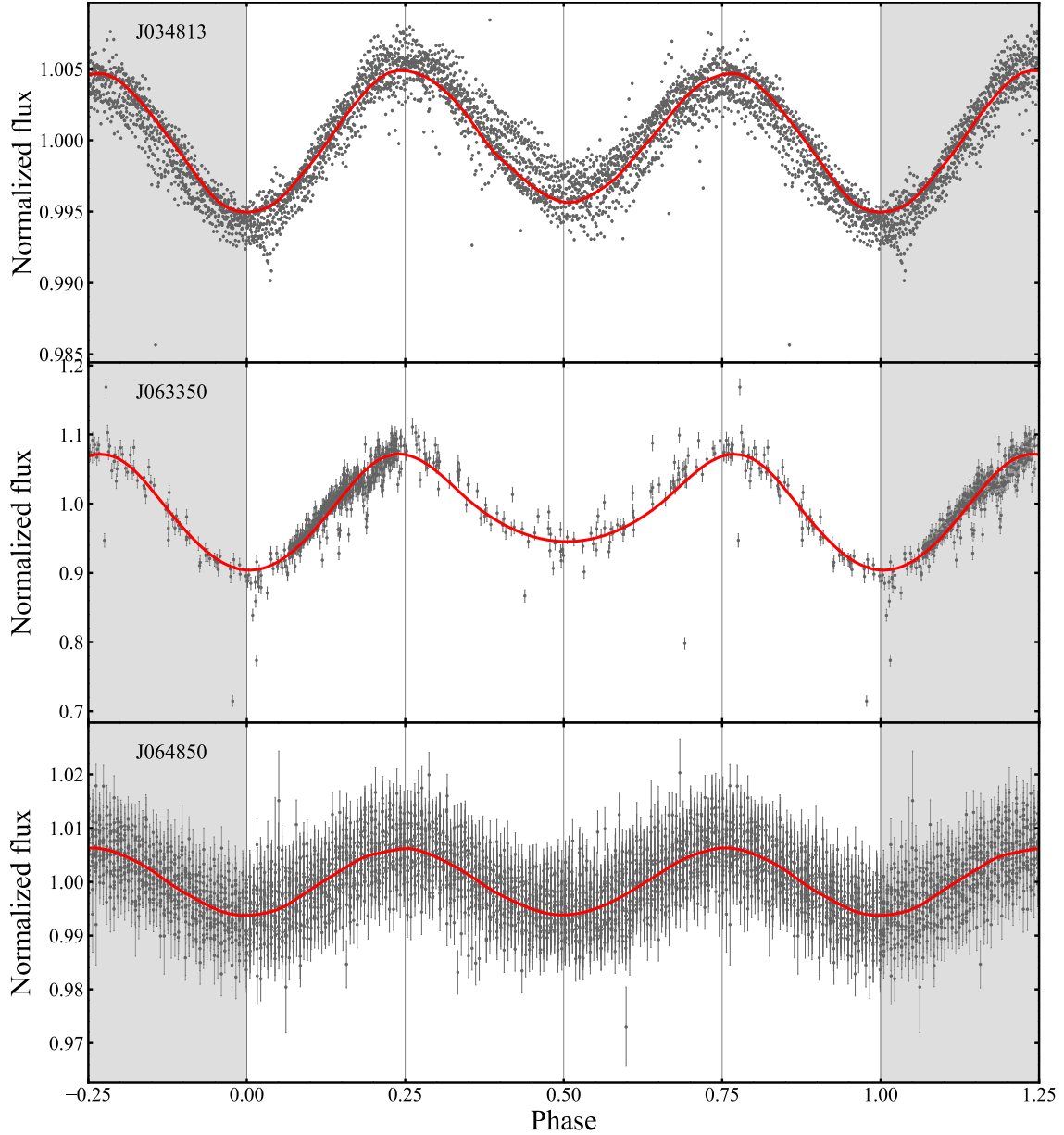


Figure 3. Light curves of three sources folded by orbital periods. The photometric data of J034813 is from K2 (The error bars for data points are invisibly small). The photometric data of J063350 is from ZTF. The photometric data of J064850 is from *TESS*. The red curve represents the best-fitting *PHOEBE* model.

with an angular distance of $0.62''$ away was reported by *Chandra*, which is a high probability X-ray counterpart of J085102. The X-ray flux is $F_{1.2-2.0\text{keV}} = 6.67^{+3.53}_{-3.73} \times 10^{-16} \text{ erg s}^{-1} \text{ cm}^{-2}$ in 1.2–2.0 keV band and $F_{0.5-7\text{keV}} = 2.26^{+1.0}_{-1.0} \times 10^{-15} \text{ erg s}^{-1} \text{ cm}^{-2}$ in 0.5–7.0 keV band. Using the distance of 0.78 kpc from *Gaia* DR3 (Gaia Collaboration et al. 2022), we convert the flux into the luminosity $L_{1.2-2.0\text{keV}} = 4.87 \times 10^{28} \text{ erg s}^{-1}$ and $L_{0.5-7\text{keV}} = 1.65 \times 10^{29} \text{ erg s}^{-1}$, for 1.2–2.0 keV band and 0.5–7.0 keV band, respectively. The X-ray luminosity of J085102 is $\sim 2 - 5$ orders of magnitude smaller than low-mass X-ray binaries in the quiescent state (La-

sota 2001; Remillard & McClintock 2006; Bernardini & Cackett 2014), which is about $10^{31-33} \text{ erg s}^{-1}$, therefore J085102 is an X-ray faint source. Notably, Wang et al. (2020) calculated the X-ray luminosity of J085102 in the 0.3–8 keV as $2 \times 10^{29} \text{ erg s}^{-1}$, and the X-ray-to-bolometric luminosity ratio is $\log R_X = -4.84$, which was considered that the X-ray emission originates from normal stellar X-ray activity.

In addition to X-ray observations, we cross-match the six candidates with GALEX using a cross-matching radius of $20''$. J063350 and J064717 are not observed by GALEX. J034813, J064850, J085102, and J104734

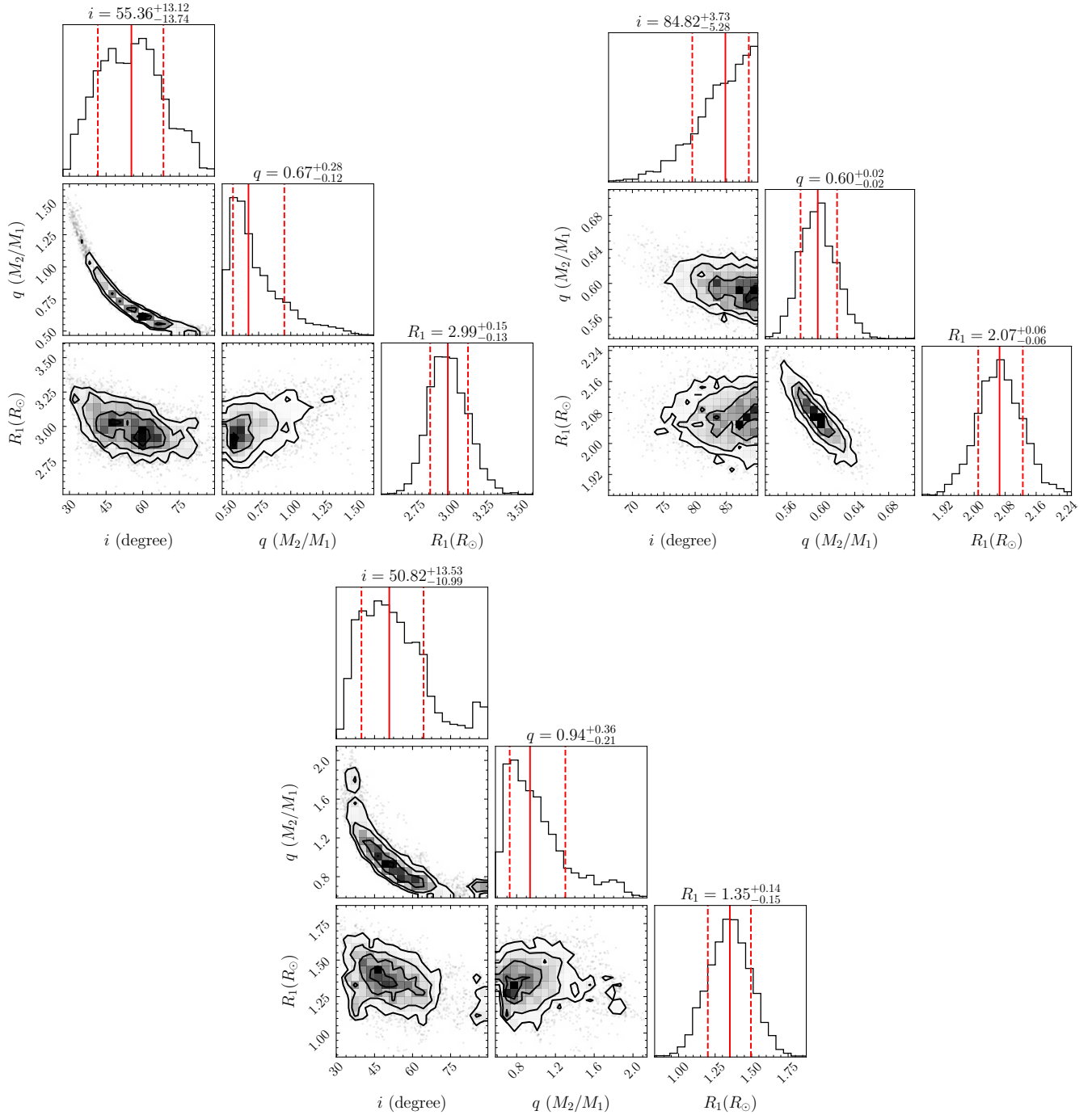


Figure 4. Parameter distributions of the light curves fitting. The top left, top right, and bottom corners correspond to J034813, J063350, and J064850, respectively.

are covered in GALEX’s footprints, but neither FUV nor NUV magnitudes are reported. The UV (non-)observations indicate the compact objects are intrinsically UV-faint; that is, they could be a cold WD or an NS. In the case of a WD, we use the GALEX detection limiting magnitude of NUV ~ 25.5 mag (Morrissey et al. 2007) and the WD cooling model (Bédard et al. 2020) to constrain the WD’s NUV flux and obtain an upper

limit of the effective temperature. The upper limits for J034813 and J064850 are 8000 K and 9500 K, respectively.

We select three binaries possibly containing unseen WDs by using the dynamical method, which is distinct from the spectroscopic decomposition method (Li et al. 2014; Rebassa-Mansergas et al. 2016) and the UV-excess selection method (Parsons et al. 2016). Since WDs in

binaries are intrinsically faint relative to the bright MS stars (e.g. F-, G-, and K-type stars), the spectral decomposition method is typically limited to finding WD–M dwarf binaries (Rebassa-Mansergas et al. 2012; Bar et al. 2017). The UV-excess method can find WD–MS binaries with bright MS companions; however, stellar chromospheric UV emission (Linsky 2017) can severely contaminate the UV-excess candidates. Moreover, the UV-excess method cannot resolve UV-faint sources similar to our candidates J034813 and J064850. In this aspect, the dynamical method is more robust since the orbital parameters and therefore the mass of the unseen compact object can be obtained.

5. SUMMARY

Based on the spectroscopic data from the LAMOST TD survey of four K2 plates (Wang et al. 2021), we propose a sample consisting of six single-lined spectroscopic binary systems that may conceal compact objects. Multi-epoch (time-resolved) spectroscopic data provide solid measurements of the stellar radial velocities. We utilize several methods to determine the orbital periods from the radial velocities, fit the radial velocity curve, and calculate the mass function. The six compact object candidates in our sample have $f(M_2) \gtrsim 0.1M_\odot$.

We use the SED fitting to estimate the stellar radius and mass. Based on the mass function and the mass of the visible star, we obtain the lower mass limit of the invisible component M_2^{\min} assuming that $i = 90^\circ$. The estimated M_2^{\min} exceeds half of the visible stellar mass for all sources. We also obtain light curves from K2, ZTF, and *TESS* surveys for three targets: J034813, J063350, and J064850, respectively. These light curves show prominent ellipsoidal variability as expected from the tidal distortion of a compact object companion. We use the PHOEBE model to constrain the orbital inclination angle and hence the mass of the unseen companion. The results indicate that these sources may be binary systems containing a massive white dwarf or neutron star.

In addition, we calculate the visible star’s Roche lobe filling factor, showing that most of the systems are not filling up their Roche lobe and therefore could be non-accreting systems. The sources exhibit no X-ray de-

tection except J085120, which is an X-ray faint source. Its X-ray emission can be attributed to stellar activity rather than accretion by the compact companion. We note that the six sources are worth follow-up observations to reveal their true nature.

Thanks to various wide-field TD spectroscopic and photometric surveys, we expect the dynamical method to potentially unearth more hidden compact objects in binary systems. Future observations of other K2 or *TESS* footprints by LAMOST will aid in expanding the sample of compact objects with a wobbling stellar companion.

We thank Jin-Bo Fu and Ling-Lin Zheng for their helpful discussions, and the anonymous referee for the constructive suggestions to improve the paper. This work was supported by the National Key R&D Program of China under grant 2021YFA1600401, the National Natural Science Foundation of China under grants 11925301, 11933004, 11988101, 12033006, 12103041, 12221003, and 12273057. This paper uses the data from the LAMOST survey. Guoshoujing Telescope (the Large Sky Area Multi-Object Fiber Spectroscopic Telescope LAMOST) is a National Major Scientific Project built by the Chinese Academy of Sciences. Funding for the project has been provided by the National Development and Reform Commission. LAMOST is operated and managed by the National Astronomical Observatories, Chinese Academy of Sciences. This paper includes data collected by the *TESS* mission and the K2 mission, which are obtained from the Mikulski Archive for Space Telescopes (MAST) at the Space Telescope Science Institute. The specific observations can be accessed via [10.17909/fwdt-2x66](https://archive.stsci.edu/fwdt-2x66) & [10.17909/T9WS3R](https://archive.stsci.edu/T9WS3R). ZTF is a public-private partnership, with equal support from the ZTF Partnership and from the U.S. National Science Foundation through the Mid-Scale Innovations Program (MSIP).

Software: astroARIADNE (Vines & Jenkins 2022), Astropy (Astropy Collaboration et al. 2013, 2018), Lightkurve (Lightkurve Collaboration et al. 2018), Matplotlib (Hunter 2007), NumPy (Harris et al. 2020), Pandas (Wes McKinney 2010), emcee (Foreman-Mackey et al. 2013), PHOEBE (Prša & Zwitter 2005; Prsa et al. 2011; Conroy et al. 2020)

REFERENCES

- Abazajian, K. N., Adelman-McCarthy, J. K., Agüeros, M. A., et al. 2009, *ApJS*, 182, 543, doi: [10.1088/0067-0049/182/2/543](https://doi.org/10.1088/0067-0049/182/2/543)
- Abbott, B. P., et al. 2016, *PhRvL*, 116, 061102, doi: [10.1103/PhysRevLett.116.061102](https://doi.org/10.1103/PhysRevLett.116.061102)
- . 2017, *ApJL*, 848, L12, doi: [10.3847/2041-8213/aa91c9](https://doi.org/10.3847/2041-8213/aa91c9)

- . 2020, *ApJL*, 892, L3, doi: [10.3847/2041-8213/ab75f5](https://doi.org/10.3847/2041-8213/ab75f5)
- Astropy Collaboration, Robitaille, T. P., Tollerud, E. J., et al. 2013, *A&A*, 558, A33, doi: [10.1051/0004-6361/201322068](https://doi.org/10.1051/0004-6361/201322068)
- Astropy Collaboration, Price-Whelan, A. M., Sipőcz, B. M., et al. 2018, *AJ*, 156, 123, doi: [10.3847/1538-3881/aabc4f](https://doi.org/10.3847/1538-3881/aabc4f)
- Bar, I., Vreeswijk, P., Gal-Yam, A., Ofek, E. O., & Nelemans, G. 2017, *ApJ*, 850, 34, doi: [10.3847/1538-4357/aa91d4](https://doi.org/10.3847/1538-4357/aa91d4)
- Bédard, A., Bergeron, P., Brassard, P., & Fontaine, G. 2020, *ApJ*, 901, 93, doi: [10.3847/1538-4357/abafbe](https://doi.org/10.3847/1538-4357/abafbe)
- Bellm, E. C., Kulkarni, S. R., Graham, M. J., et al. 2019, *PASP*, 131, 018002, doi: [10.1088/1538-3873/aaecbe](https://doi.org/10.1088/1538-3873/aaecbe)
- Bernardini, F., & Cackett, E. M. 2014, *MNRAS*, 439, 2771, doi: [10.1093/mnras/stu140](https://doi.org/10.1093/mnras/stu140)
- Bianchi, L., Herald, J., Efremova, B., et al. 2011, *Ap&SS*, 335, 161, doi: [10.1007/s10509-010-0581-x](https://doi.org/10.1007/s10509-010-0581-x)
- Brown, G. E., & Bethe, H. A. 1994, *ApJ*, 423, 659, doi: [10.1086/173844](https://doi.org/10.1086/173844)
- Casares, J., Negueruela, I., Ribó, M., et al. 2014, *Nature*, 505, 378, doi: [10.1038/nature12916](https://doi.org/10.1038/nature12916)
- Chambers, K. C., Magnier, E. A., Metcalfe, N., et al. 2016, arXiv e-prints, arXiv:1612.05560. <https://arxiv.org/abs/1612.05560>
- Claret, A., & Bloemen, S. 2011, *A&A*, 529, A75, doi: [10.1051/0004-6361/201116451](https://doi.org/10.1051/0004-6361/201116451)
- Conroy, K. E., Kochoska, A., Hey, D., et al. 2020, *ApJS*, 250, 34, doi: [10.3847/1538-4365/abb4e2](https://doi.org/10.3847/1538-4365/abb4e2)
- Corral-Santana, J. M., Casares, J., Muñoz-Darias, T., et al. 2016, *A&A*, 587, A61, doi: [10.1051/0004-6361/201527130](https://doi.org/10.1051/0004-6361/201527130)
- . 2013, *Science*, 339, 1048, doi: [10.1126/science.1228222](https://doi.org/10.1126/science.1228222)
- Cui, X.-Q., Zhao, Y.-H., Chu, Y.-Q., et al. 2012, *Research in Astronomy and Astrophysics*, 12, 1197, doi: [10.1088/1674-4527/12/9/003](https://doi.org/10.1088/1674-4527/12/9/003)
- Dotter, A. 2016, *ApJS*, 222, 8, doi: [10.3847/0067-0049/222/1/8](https://doi.org/10.3847/0067-0049/222/1/8)
- Duchêne, G., & Kraus, A. 2013, *ARA&A*, 51, 269, doi: [10.1146/annurev-astro-081710-102602](https://doi.org/10.1146/annurev-astro-081710-102602)
- El-Badry, K., Quataert, E., Rix, H.-W., et al. 2021a, *MNRAS*, 505, 2051, doi: [10.1093/mnras/stab1318](https://doi.org/10.1093/mnras/stab1318)
- . 2021b, *MNRAS*, 505, 2051, doi: [10.1093/mnras/stab1318](https://doi.org/10.1093/mnras/stab1318)
- El-Badry, K., Rix, H.-W., Quataert, E., et al. 2022, *MNRAS*, doi: [10.1093/mnras/stac3140](https://doi.org/10.1093/mnras/stac3140)
- El-Badry, K., Rix, H.-W., Cendes, Y., et al. 2023, arXiv e-prints, arXiv:2302.07880, doi: [10.48550/arXiv.2302.07880](https://doi.org/10.48550/arXiv.2302.07880)
- Evans, I. N., Primi, F. A., Glotfelty, K. J., et al. 2010, *ApJS*, 189, 37, doi: [10.1088/0067-0049/189/1/37](https://doi.org/10.1088/0067-0049/189/1/37)
- Foreman-Mackey, D., Hogg, D. W., Lang, D., & Goodman, J. 2013, *PASP*, 125, 306, doi: [10.1086/670067](https://doi.org/10.1086/670067)
- Fu, J.-N., Cat, P. D., Zong, W., et al. 2020, *Research in Astronomy and Astrophysics*, 20, 167, doi: [10.1088/1674-4527/20/10/167](https://doi.org/10.1088/1674-4527/20/10/167)
- Gaia Collaboration, Vallenari, A., Brown, A. G. A., et al. 2022, arXiv e-prints, arXiv:2208.00211. <https://arxiv.org/abs/2208.00211>
- Gomel, R., Faigler, S., & Mazeh, T. 2021, *MNRAS*, 501, 2822, doi: [10.1093/mnras/staa3305](https://doi.org/10.1093/mnras/staa3305)
- Gomel, R., Mazeh, T., Faigler, S., et al. 2022, arXiv e-prints, arXiv:2206.06032. <https://arxiv.org/abs/2206.06032>
- Gu, W.-M., Mu, H.-J., Fu, J.-B., et al. 2019, *ApJL*, 872, L20, doi: [10.3847/2041-8213/ab04f0](https://doi.org/10.3847/2041-8213/ab04f0)
- Harris, C. R., Millman, K. J., van der Walt, S. J., et al. 2020, *Nature*, 585, 357, doi: [10.1038/s41586-020-2649-2](https://doi.org/10.1038/s41586-020-2649-2)
- Henden, A., & Munari, U. 2014, *Contributions of the Astronomical Observatory Skalnaté Pleso*, 43, 518
- Howell, S. B., Sobek, C., Haas, M., et al. 2014, *PASP*, 126, 398, doi: [10.1086/676406](https://doi.org/10.1086/676406)
- Hunter, J. D. 2007, *Computing in Science & Engineering*, 9, 90, doi: [10.1109/MCSE.2007.55](https://doi.org/10.1109/MCSE.2007.55)
- Jayasinghe, T., Stanek, K. Z., Thompson, T. A., et al. 2021, *MNRAS*, 504, 2577, doi: [10.1093/mnras/stab907](https://doi.org/10.1093/mnras/stab907)
- Joss, P. C., & Rappaport, S. A. 1984, *ARA&A*, 22, 537, doi: [10.1146/annurev.aa.22.090184.002541](https://doi.org/10.1146/annurev.aa.22.090184.002541)
- Kreidberg, L., Bailyn, C. D., Farr, W. M., & Kalogera, V. 2012, *ApJ*, 757, 36, doi: [10.1088/0004-637X/757/1/36](https://doi.org/10.1088/0004-637X/757/1/36)
- Lasota, J.-P. 2001, *NewAR*, 45, 449, doi: [10.1016/S1387-6473\(01\)00112-9](https://doi.org/10.1016/S1387-6473(01)00112-9)
- Li, C.-q., Shi, J.-r., Yan, H.-l., et al. 2021, *ApJS*, 256, 31, doi: [10.3847/1538-4365/ac22a8](https://doi.org/10.3847/1538-4365/ac22a8)
- Li, L., Zhang, F., Han, Q., Kong, X., & Gong, X. 2014, *MNRAS*, 445, 1331, doi: [10.1093/mnras/stu1798](https://doi.org/10.1093/mnras/stu1798)
- Li, X., Wang, S., Zhao, X., et al. 2022, *ApJ*, 938, 78, doi: [10.3847/1538-4357/ac8f29](https://doi.org/10.3847/1538-4357/ac8f29)
- Lightkurve Collaboration, Cardoso, J. V. d. M., Hedges, C., et al. 2018, *Lightkurve: Kepler and TESS time series analysis in Python*, *Astrophysics Source Code Library*, record ascl:1812.013. <http://ascl.net/1812.013>
- Linsky, J. L. 2017, *ARA&A*, 55, 159, doi: [10.1146/annurev-astro-091916-055327](https://doi.org/10.1146/annurev-astro-091916-055327)
- Liu, J., Zhang, H., Howard, A. W., et al. 2019, *Nature*, 575, 618, doi: [10.1038/s41586-019-1766-2](https://doi.org/10.1038/s41586-019-1766-2)
- Liu, J., Zheng, Z., Soria, R., et al. 2020, *ApJ*, 900, 42, doi: [10.3847/1538-4357/aba49e](https://doi.org/10.3847/1538-4357/aba49e)
- Lomb, N. R. 1976, *Ap&SS*, 39, 447, doi: [10.1007/BF00648343](https://doi.org/10.1007/BF00648343)

- Marsh, T. R., Robinson, E. L., & Wood, J. H. 1994, MNRAS, 266, 137, doi: [10.1093/mnras/266.1.137](https://doi.org/10.1093/mnras/266.1.137)
- Martin, D. C., Fanson, J., Schiminovich, D., et al. 2005, ApJL, 619, L1, doi: [10.1086/426387](https://doi.org/10.1086/426387)
- Mazeh, T., Faigler, S., Bashi, D., et al. 2022, MNRAS, 517, 4005, doi: [10.1093/mnras/stac2853](https://doi.org/10.1093/mnras/stac2853)
- Merle, T., Van Eck, S., Jorissen, A., et al. 2017, A&A, 608, A95, doi: [10.1051/0004-6361/201730442](https://doi.org/10.1051/0004-6361/201730442)
- Morrissey, P., Conrow, T., Barlow, T. A., et al. 2007, ApJS, 173, 682, doi: [10.1086/520512](https://doi.org/10.1086/520512)
- Mu, H.-J., Gu, W.-M., Yi, T., et al. 2022, Science China Physics, Mechanics, and Astronomy, 65, 229711, doi: [10.1007/s11433-021-1809-8](https://doi.org/10.1007/s11433-021-1809-8)
- Paczynski, B. 1971, ARA&A, 9, 183, doi: [10.1146/annurev.aa.09.090171.001151](https://doi.org/10.1146/annurev.aa.09.090171.001151)
- Parsons, S. G., Rebassa-Mansergas, A., Schreiber, M. R., et al. 2016, MNRAS, 463, 2125, doi: [10.1093/mnras/stw2143](https://doi.org/10.1093/mnras/stw2143)
- Price-Whelan, A. M., Hogg, D. W., Foreman-Mackey, D., & Rix, H.-W. 2017, ApJ, 837, 20, doi: [10.3847/1538-4357/aa5e50](https://doi.org/10.3847/1538-4357/aa5e50)
- Prsa, A., Matijevic, G., Latkovic, O., Vilardell, F., & Wils, P. 2011, PHOEBE: PHysics Of Eclipsing BinariEs, Astrophysics Source Code Library, record ascl:1106.002. <http://ascl.net/1106.002>
- Prša, A., & Zwitter, T. 2005, ApJ, 628, 426, doi: [10.1086/430591](https://doi.org/10.1086/430591)
- Rebassa-Mansergas, A., Nebot Gómez-Morán, A., Schreiber, M. R., et al. 2012, MNRAS, 419, 806, doi: [10.1111/j.1365-2966.2011.19923.x](https://doi.org/10.1111/j.1365-2966.2011.19923.x)
- Rebassa-Mansergas, A., Ren, J. J., Parsons, S. G., et al. 2016, MNRAS, 458, 3808, doi: [10.1093/mnras/stw554](https://doi.org/10.1093/mnras/stw554)
- Rebassa-Mansergas, A., Solano, E., Jiménez-Esteban, F. M., et al. 2021, MNRAS, 506, 5201, doi: [10.1093/mnras/stab2039](https://doi.org/10.1093/mnras/stab2039)
- Remillard, R. A., & McClintock, J. E. 2006, ARA&A, 44, 49, doi: [10.1146/annurev.astro.44.051905.092532](https://doi.org/10.1146/annurev.astro.44.051905.092532)
- Ren, J. J., Rebassa-Mansergas, A., Parsons, S. G., et al. 2018, MNRAS, 477, 4641, doi: [10.1093/mnras/sty805](https://doi.org/10.1093/mnras/sty805)
- Ricker, G. R., Winn, J. N., Vanderspek, R., et al. 2015, Journal of Astronomical Telescopes, Instruments, and Systems, 1, 014003, doi: [10.1117/1.JATIS.1.1.014003](https://doi.org/10.1117/1.JATIS.1.1.014003)
- Rowan, D. M., Stanek, K. Z., Jayasinghe, T., et al. 2021, MNRAS, 507, 104, doi: [10.1093/mnras/stab2126](https://doi.org/10.1093/mnras/stab2126)
- Scargle, J. D. 1981, ApJS, 45, 1, doi: [10.1086/190706](https://doi.org/10.1086/190706)
- Shappee, B. J., Prieto, J. L., Grupe, D., et al. 2014, ApJ, 788, 48, doi: [10.1088/0004-637X/788/1/48](https://doi.org/10.1088/0004-637X/788/1/48)
- Skrutskie, M. F., Cutri, R. M., Stiening, R., et al. 2006, AJ, 131, 1163, doi: [10.1086/498708](https://doi.org/10.1086/498708)
- Stassun, K. G., Oelkers, R. J., Paegert, M., et al. 2019, AJ, 158, 138, doi: [10.3847/1538-3881/ab3467](https://doi.org/10.3847/1538-3881/ab3467)
- Steehhs, D., McClintock, J. E., Parsons, S. G., et al. 2013, ApJ, 768, 185, doi: [10.1088/0004-637X/768/2/185](https://doi.org/10.1088/0004-637X/768/2/185)
- Thompson, T. A., Kochanek, C. S., Stanek, K. Z., et al. 2019, Science, 366, 637, doi: [10.1126/science.aau4005](https://doi.org/10.1126/science.aau4005)
- Traulsen, I., Schwöpe, A. D., Lamer, G., et al. 2020, A&A, 641, A137, doi: [10.1051/0004-6361/202037706](https://doi.org/10.1051/0004-6361/202037706)
- Trimble, V. L., & Thorne, K. S. 1969, ApJ, 156, 1013, doi: [10.1086/150032](https://doi.org/10.1086/150032)
- Troja, E., Fryer, C. L., O'Connor, B., et al. 2022, Nature, 612, 228, doi: [10.1038/s41586-022-05327-3](https://doi.org/10.1038/s41586-022-05327-3)
- Vines, J. I., & Jenkins, J. S. 2022, MNRAS, 513, 2719, doi: [10.1093/mnras/stac956](https://doi.org/10.1093/mnras/stac956)
- Voges, W., Aschenbach, B., Boller, T., et al. 1999, A&A, 349, 389. <https://arxiv.org/abs/astro-ph/9909315>
- Wang, S., Bai, Y., He, L., & Liu, J. 2020, ApJ, 902, 114, doi: [10.3847/1538-4357/abb66d](https://doi.org/10.3847/1538-4357/abb66d)
- Wang, S., Zhang, H.-T., Bai, Z.-R., et al. 2021, Research in Astronomy and Astrophysics, 21, 292, doi: [10.1088/1674-4527/21/11/292](https://doi.org/10.1088/1674-4527/21/11/292)
- Wes McKinney. 2010, in Proceedings of the 9th Python in Science Conference, ed. Stéfan van der Walt & Jarrod Millman, 56 – 61, doi: [10.25080/Majora-92bf1922-00a](https://doi.org/10.25080/Majora-92bf1922-00a)
- Wright, E. L., Eisenhardt, P. R. M., Mainzer, A. K., et al. 2010, AJ, 140, 1868, doi: [10.1088/0004-6256/140/6/1868](https://doi.org/10.1088/0004-6256/140/6/1868)
- Yang, F., Zhang, B., Long, R. J., et al. 2021, ApJ, 923, 226, doi: [10.3847/1538-4357/ac31b3](https://doi.org/10.3847/1538-4357/ac31b3)
- Yi, T., Gu, W.-M., Zhang, Z.-X., et al. 2022, Nature Astronomy, doi: [10.1038/s41550-022-01766-0](https://doi.org/10.1038/s41550-022-01766-0)
- Yuan, H., Wang, S., Bai, Z., et al. 2022, ApJ, 940, 165, doi: [10.3847/1538-4357/ac9c62](https://doi.org/10.3847/1538-4357/ac9c62)
- Zhang, Z.-X., Zheng, L.-L., Gu, W.-M., et al. 2022, ApJ, 933, 193, doi: [10.3847/1538-4357/ac75b6](https://doi.org/10.3847/1538-4357/ac75b6)
- Zheng, L.-L., Gu, W.-M., Yi, T., et al. 2019, AJ, 158, 179, doi: [10.3847/1538-3881/ab449f](https://doi.org/10.3847/1538-3881/ab449f)
- Zheng, L.-L., Gu, W.-M., Sun, M., et al. 2022a, ApJ, 936, 33, doi: [10.3847/1538-4357/ac853f](https://doi.org/10.3847/1538-4357/ac853f)
- Zheng, L.-L., Sun, M., Gu, W.-M., et al. 2022b, arXiv e-prints, arXiv:2210.04685. <https://arxiv.org/abs/2210.04685>
- Zong, W., Fu, J.-N., De Cat, P., et al. 2020, ApJS, 251, 15, doi: [10.3847/1538-4365/abbb2d](https://doi.org/10.3847/1538-4365/abbb2d)

APPENDIX

To verify that the systems are single-lined spectroscopic binaries, we checked whether the CCF profile has a single peak, an indication of a single dominant component. We adopt two spectra for each target source to compute the CCF. These two spectra are chosen to be mostly in anti-orbital phases (near the quadrature phases), such that if there are two components, they would be easily detected in the velocity space. J104734 has poor SNR for most of the spectra, therefore we trade off the phase requirement for better SNR. J063350 and J064850 also have poor medium-resolution spectra, therefore we turn to use the low-resolution spectra. The results the Figure 5 suggest that these sources are most likely single-lined binaries given the current spectroscopic resolution.

Figure 6 presents the broadband SED fitting of three targets with ellipsoidal light curve variations. The fitting is performed using the `astroARIADNE` (Vines & Jenkins 2022) with a single stellar component model. The results suggest that these three targets can be well-fitted with the SED model; No evidence of contamination from other components supports our conclusions about the nature of these systems.

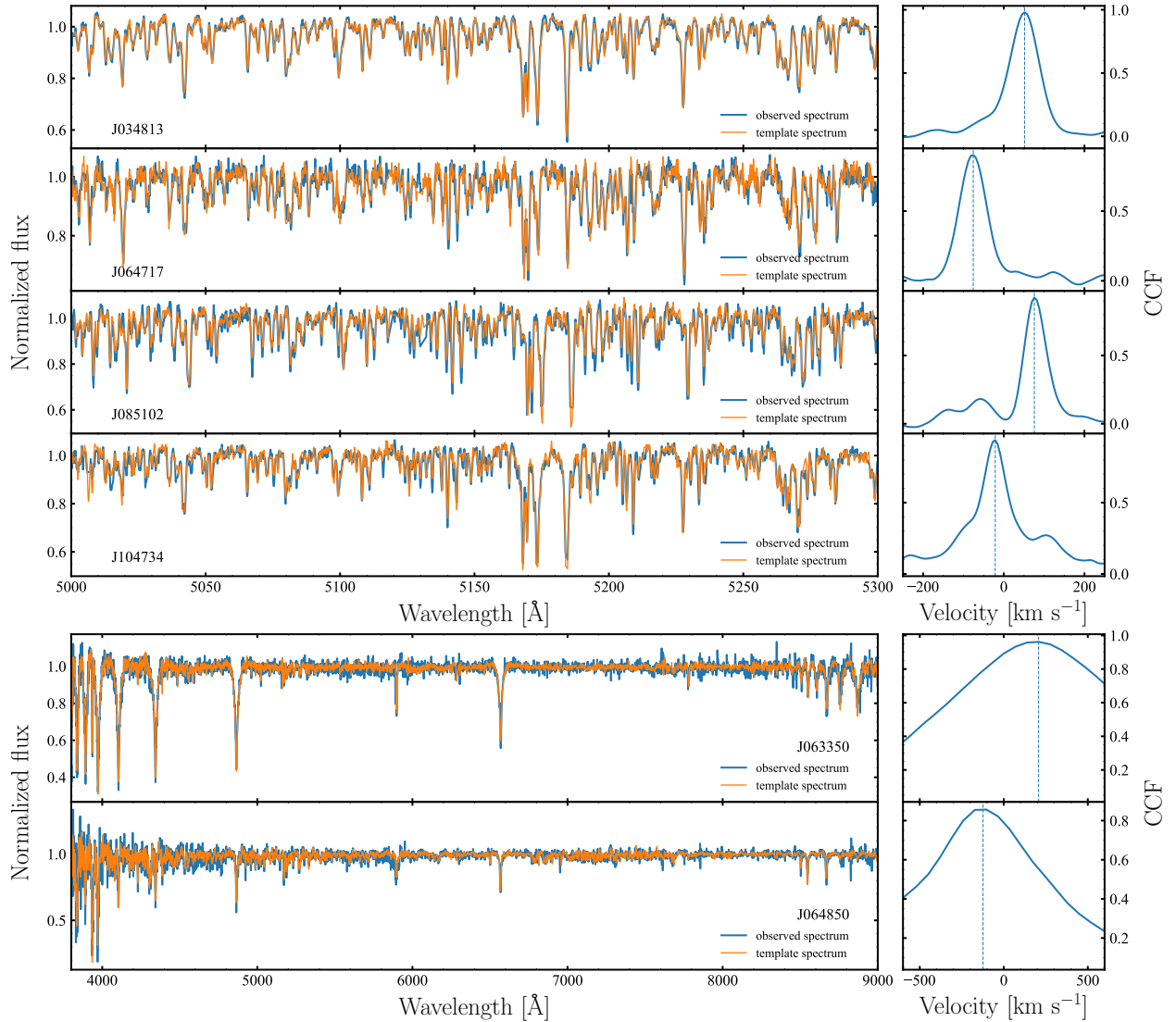


Figure 5. LAMOST spectra (left panels) and CCF profile (right panels) for the candidates. In each left panel, two spectra used to perform the CCF are both observational spectra but are styled with distinct colors and labels to indicate which one is used as the template. The vertical dashed lines in the right panels indicate the measured (relative) radial velocity.

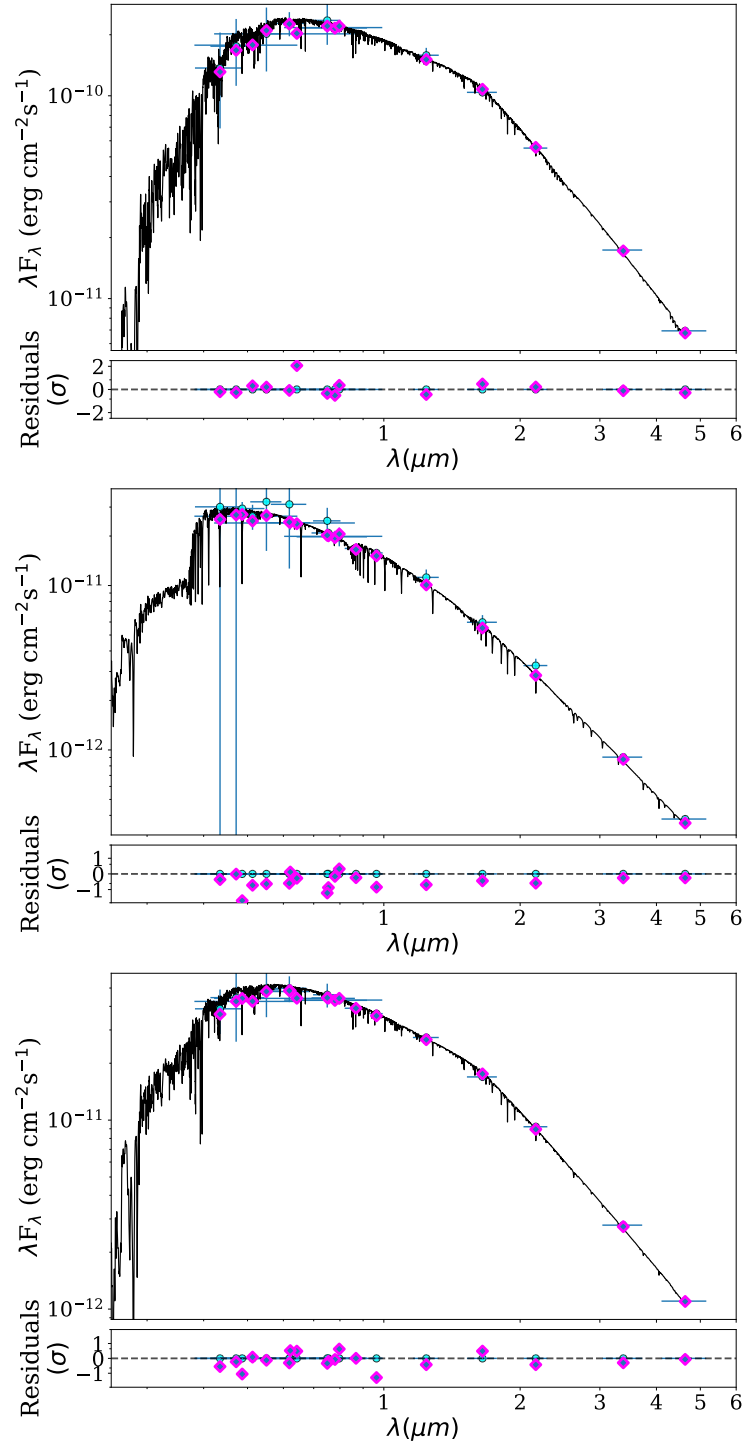


Figure 6. The SED fitting results of J034813 (top panel), J063350 (middle panel), and J064850 (bottom panel). Cyan points are the observed fluxes, purple diamonds are the synthetic fluxes, and the black curve is the best-fit SED model.